The chemistry of extragalactic carbon stars

Paul M. Woods,[1,2]★ C. Walsh,[3] M. A. Cordiner[4] and F. Kemper[5]

[1]*Department of Physics & Astronomy, University College London, Gower Street, London WC1E 6BT*
[2]*Jodrell Bank Centre for Astrophysics, Alan Turing Building, School of Physics and Astronomy, The University of Manchester, Oxford Road, Manchester M13 9PL*
[3]*Astrophysics Research Centre, School of Mathematics & Physics, Queen's University Belfast, University Road, Belfast BT7 1NN*
[4]*Astrochemistry Laboratory and The Goddard Center for Astrobiology, NASA Goddard Space Flight Center, Code 691, 8800 Greenbelt Road, Greenbelt MD 20771, USA*
[5]*Academia Sinica Institute of Astronomy & Astrophysics, PO Box 23-141, Taipei 10617, Taiwan*

ABSTRACT

Prompted by the ongoing interest in *Spitzer* Infrared Spectrometer spectra of carbon stars in the Large Magellanic Cloud, we have investigated the circumstellar chemistry of carbon stars in low-metallicity environments. Consistent with observations, our models show that acetylene is particularly abundant in the inner regions of low metallicity carbon-rich asymptotic giant branch stars – more abundant than carbon monoxide. As a consequence, larger hydrocarbons have higher abundances at the metallicities of the Magellanic Clouds than in stars with solar metallicity. We also find that the oxygen and nitrogen chemistry is suppressed at lower metallicity, as expected. Finally, we calculate molecular line emission from carbon stars in the Large and Small Magellanic Cloud and find that several molecules should be readily detectable with the Atacama Large Millimeter Array at Full Science operations.

Key words: Astrochemistry – stars: AGB and post-AGB – stars: carbon – circumstellar matter – infrared: stars – submillimetre: stars.

1 INTRODUCTION

The advent of the Atacama Large Millimeter Array (ALMA) and other large (sub-)millimetre telescopes, with their unprecedented spatial resolution and sensitivity, will allow the observation of giant stars in other galaxies in similar detail to that achieved for Galactic objects. These advanced capabilities prompt investigation into the nature of these extragalactic stars, with one of the most interesting aspects being the study of the effect of sub-solar metallicities on circumstellar chemistry and dust composition.

Recent studies in the infrared using the *Spitzer Space Telescope* and ground-based instruments have highlighted the deep molecular absorption of, primarily, acetylene in the spectra of evolved carbon stars, in the Magellanic Clouds (MCs; e.g. van Loon, Zijlstra & Groenewegen 1999a; Matsuura et al. 2002, 2005; van Loon 2006; Sloan et al. 2006; Speck et al. 2006; Zijlstra et al. 2006; Lagadec et al. 2007; Leisenring, Kemper & Sloan 2008; van Loon et al. 2008; Woods et al. 2011, etc.). These absorption features are in general deeper than those seen in Galactic stars, and this implies that there is a difference between the chemistry of Magellanic circumstellar envelopes (CSEs) and Galactic carbon stars, which are comparatively well studied.

The MCs are nearby dwarf galaxies with sub-solar metallicities. The Large Magellanic Cloud (LMC), at a distance of ∼50 kpc

(Schaefer 2008), has an average metallicity of around 50 per cent solar (Dufour, Shields & Talbot 1982; Westerlund 1997). The Small Magellanic Cloud (SMC), at a slightly larger distance of 66 kpc (Szewczyk et al. 2009), has an average metallicity of 20 per cent solar (Dufour et al. 1982; Westerlund 1997). The effect of this low metallicity regime on dust composition and galactic dust budgets has been studied observationally by many authors (e.g. Zijlstra et al. 2006; Lagadec et al. 2007; van Loon et al. 2008; Matsuura et al. 2009). However, the effects on circumstellar chemistry have not been, as yet, studied in any detail, and our aim here is to pioneer in the field with this work.

The chemical modelling of Galactic asymptotic giant branch (AGB) stars was first attempted 35 years ago. Initial attempts focused on simple physical models and chemistry appropriate for oxygen-rich ($n(O) > n(C)$) circumstellar environments (Goldreich & Scoville 1976; Scalo & Slavsky 1980; Jura & Morris 1981). Physical models have largely remained simple (with some notable exceptions, e.g. Cordiner & Millar 2009) whereas the chemical modelling has moved to focus on carbon-rich ($n(C) > n(O)$) circumstellar chemistry since it shows a wider variety of molecules (e.g. Huggins & Glassgold 1982). Progress in chemical modelling is driven in part by the desire to explain observed abundances of newly detected molecules in the most accessible carbon star, IRC+10216, for instance, in the addition of long carbon-chain molecules (Millar, Herbst & Bettens 2000) or anion species (Millar et al. 2007). In this case, advances in technology have driven us to investigate carbon-rich circumstellar chemistry in previously challenging locations.

★E-mail: paul.woods@ucl.ac.uk

In this paper, we present the results of modelling the circumstellar chemistry around carbon-rich AGB stars at sub-solar metallicities. We focus on three fiducial models, at metallicities and with physical conditions appropriate for the Galaxy, the LMC and the SMC. We initially assume solar metallicity ($Z = 0.02$) for Galactic carbon stars, and average interstellar metallicities for LMC ($Z = 0.008$) and SMC ($Z = 0.004$) carbon stars. In Section 2, we describe our adopted physical model and discuss the different physical and chemical considerations, and also discuss sources of uncertainties in our models in Section 2.6. In Section 3, we describe how we calculate the chemical evolution of the CSE. We show our results in Section 4, preceding a discussion in Section 5 (including our calculations of molecular line emission which may be observable with ALMA) and finally, in Section 6, we draw our conclusions regarding the chemistry of low-metallicity carbon stars.

2 CHEMICAL AND PHYSICAL CONSIDERATIONS AT LOW METALLICITY

Nucleosynthetic products dredged (via convection) from the stellar interior are mixed to the surface of the star, where material is accelerated to the terminal velocity of the stellar wind within a radius of $20\,R_\star$ (Keady, Hall & Ridgway 1988) and passed into the CSE. The gas, which is mainly molecular hydrogen, is well mixed with dust grains. We assume a spherical geometry where the gas has a $1/R^2$ density distribution, and a temperature profile which follows:

$$T(r) = \max[150(R/R_0)^{-0.79};\ 10]\,K \quad (R \geq R_0 = 5 \times 10^{15}\,cm)$$

(e.g. Millar & Herbst 1994; Millar et al. 2000). The CSE is irradiated by the interstellar radiation field (ISRF), but not by ultraviolet (UV) photons from the star itself, which are quenched in the stellar atmosphere. Extinction in the CSE is calculated according to the approach of Jura & Morris (1981), assuming interstellar-type grains, and we treat CO self-shielding according to Mamon, Glassgold & Huggins (1988). We model the carbon-rich chemistry in the circumstellar region between $\sim$200 and $100\,000\,R_\star$ (0.005–3×10^{18} cm).

In the subsequent sections, we consider the chemical and further physical ingredients of our model. Observationally, very little is known about the chemistry of extragalactic carbon stars, and so we mainly discuss the chemistry of Galactic carbon stars, using the nucleosynthesis models of Karakas (2010) to adjust for lower metallicities (see Section 2.1). Physical parameters of LMC and SMC carbon stars are more well constrained observationally, and we summarize those aspects in Sections 2.2–2.5.

2.1 Initial chemical abundances

As circumstellar material cools during the expansion of the stellar wind, it is energetically favourable for atomic elements to form molecules in the photosphere of the star ($R \lesssim 5\,R_\star$), where the chemistry is in thermal equilibrium (TE) due to the high temperatures and densities. For molecules of high stability, that is to say, those which contain strong internal bonds, the abundances amounted in this region of the star are carried through into the non-TE outer envelope ($R \gtrsim 100\,R_\star$) without significant change. In carbon-rich environments, such molecules include CO, N_2, HCN and C_2H_2 (e.g. Tsuji 1973; Millar 2008).

A further group of molecules are also observed at high abundances at the inner edge of the outer envelope in Galactic stars. This subset is generally formed at low abundance in the TE photosphere of the star, but attains a higher abundance in the inner envelope

where dust is formed and then accelerated ($5 \lesssim R \lesssim 100\,R_\star$) due to non-equilibrium processes. They comprise CS, SiO, SiS, NH_3, SiH_4 and CH_4 (e.g. Cherchneff 2006). These two subsets of molecules are often called 'parent species'.

To obtain accurate initial abundances for these 10 parent species when modelling the chemistry in the outer envelope ($R \gtrsim 100\,R_\star$) at different metallicities, one must employ different techniques for the two subsets of parents. For the high stability parent species, we can use a TE model to calculate the relevant data. This approach has been used previously to good effect (e.g. Tsuji 1973; Sharp & Huebner 1990; Markwick 2000). For the remaining parent species, other physical factors must be taken into consideration, such as depletion through dust formation (SiS, SiO; Bieging & Nguyen-Quang-Rieu 1989; Schöier et al. 2006), pulsation-driven shocks (SiS, SiO, CS; Willacy & Cherchneff 1998) and gas–grain interaction (e.g. hydrogenation leading to NH_3, SiH_4 and CH_4). Modelling these complexities in detail, which indeed themselves have been the subject of much investigation, is too advanced for this initial study and thus we must use other arguments discussed below.

2.1.1 TE molecules (CO, N_2, C_2H_2, HCN)

The TE model used is similar to that detailed by Sharp & Huebner (1990) and Markwick (2000),[1] which work by minimizing the Gibbs free energy of the thermodynamic system. We adopt a temperature of 2250 K and a pressure of 1.033×10^{-3} atm, appropriate for the photosphere of a carbon-rich AGB star (Ivezić & Elitzur 1996; Markwick 2000). Results of the TE calculations for the range of temperatures 2500–2000 K are displayed in Fig. 1; those species for which TE is appropriate are largely invariant across the temperature range. Elemental abundances for AGB stars at different metallicities are taken from the nucleosynthesis calculations of Karakas (2010) for a $3\,M_\odot$ star. This mass was chosen because it was the lowest mass model for which the star became carbon rich at the three metallicities $Z = 0.02$ (Galaxy), $Z = 0.008$ (LMC) and $Z = 0.004$ (SMC). There are incongruities with these models, in that it is clear from observational evidence that carbon stars in the Milky Way (MW) can form at masses as low as $\sim$1.5$\,M_\odot$ (Wallerstein & Knapp 1998). These modelling issues are acknowledged and being addressed (Karakas 2011), and we continue to use the results since they are a consistent set of readily available abundances. Average stellar yields were used as inputs for the TE model and the resulting fractional abundances with respect to H_2 can be found in Table 1 for CO, N_2, C_2H_2 and HCN. This method (using the results of nucleosynthesis calculations) is preferable to using the elemental abundances of the MCs in general, since much of the circumstellar chemistry depends on the amount of carbon generated by the star in the AGB phase (Matsuura et al. 2008). In the next section, we describe our method of determining input abundances for those molecules for which TE does not apply. Table 3 summarises the physical parameters discussed in Section 2.2–2.5.

2.1.2 Non-TE molecules (CS, SiO, SiS, NH_3, SiH_4, CH_4)

The observed distribution of SiO peaks within a few stellar radii in the archetypal carbon star, IRC+10216 (Keady & Ridgway 1993; Schöier et al. 2006). SiO is seen at high fractional abundances, $n(SiO)/n(H_2) \sim 10^{-6}$, whereas TE models underpredict the abundance by around a factor of 30. Its formation is thought to be due to

---

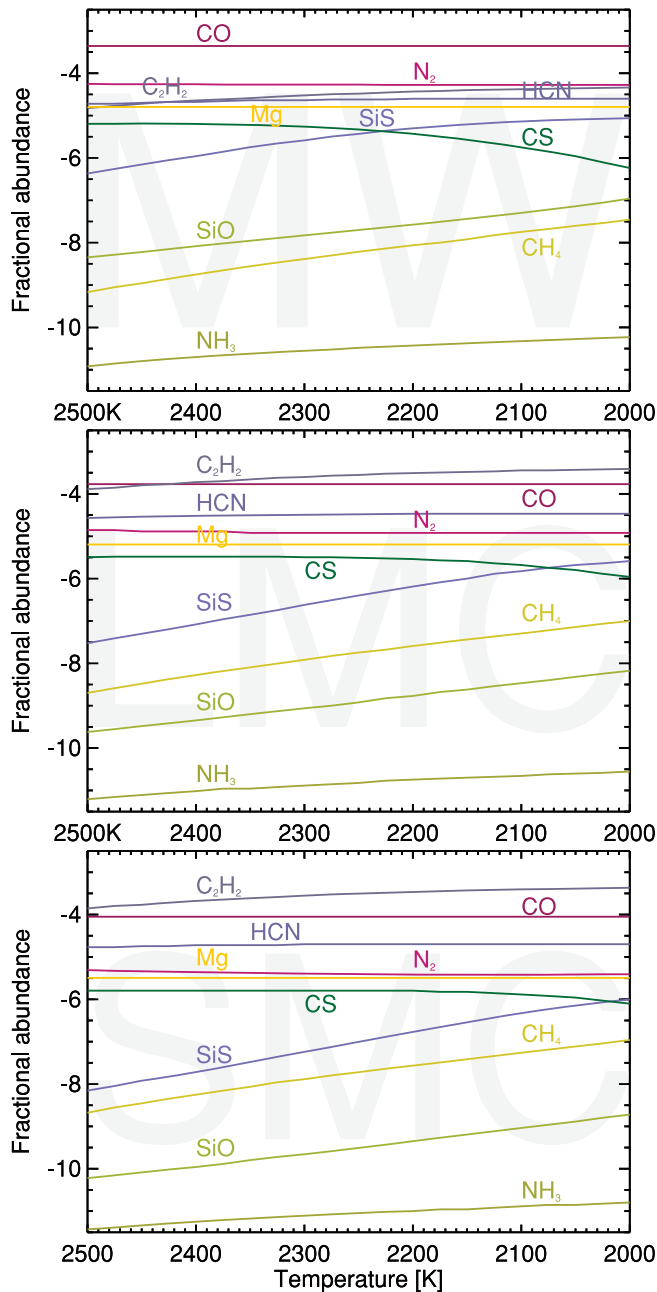[1] Available on request to the authors.

Figure 1. Fractional abundances (log scale) at TE for MW, LMC and SMC metallicities, at a pressure of $P \sim 10^{-3}$ atm. We utilize values at 2250 K in the subsequent modelling.

circumstellar shocks, and hence its abundance is dependent on that of atomic oxygen, since in the shocked material the reaction

$$Si + OH \longrightarrow SiO + H \qquad (1)$$

dominates (Hartquist, Dalgarno & Oppenheimer 1980; Willacy & Cherchneff 1998). As such, we choose to set the fractional abundance of SiO to $10^{-3} n(O)$, in line with that observed in IRC+10216.

SiS is the main repository for both silicon and sulphur in the gas phase, and forms at a high abundance in TE models. Observations indicate that it is rapidly depleted as gas flows through the intermediate envelope, presumably due to the adsorption of the molecule on to grain surfaces (Bieging & Nguyen-Quang-Rieu 1989; Boyle et al. 1994). Thus, we assume that the initial abundance of SiS is equal to the elemental abundance of sulphur minus the fraction of CS

(discussed below). For IRC+10216, this premise agrees well with observations (Bieging & Tafalla 1993; Lucas et al. 1995; Schöier et al. 2006; Decin et al. 2010).

CS is slightly overproduced in TE models compared to observations (Keady & Ridgway 1993) and the work by Willacy & Cherchneff (1998) has shown that CS is destroyed by pulsation-driven shocks by a considerable amount, the extent of which depends on the assumed shock speed. It then slowly reforms in the outflowing wind. We assume slow shock speeds ($10\,\mathrm{km\,s^{-1}}$) and the same shock-destruction efficiency as that of Willacy & Cherchneff (1998), and adopt an abundance of CS a factor of 2 less than its TE abundance.

Emission from the hydrogenated species NH_3, CH_4 and SiH_4 originates in the dust-formation zone and inner envelope around IRC+10216 (Keady & Ridgway 1993). Although surprising because of the high temperature of the dust in these regions, these molecules are most likely formed via hydrogen-addition reactions on the surface of dust grains. The very short time-scale before ejection from the grain surface would indicate that hydrogen is the dominant reaction partner for adsorbed atoms. Typically these molecules are of low abundance in both TE (e.g. Tsuji 1964) and non-TE models (Willacy & Cherchneff 1998, and others), adding further weight to grain-surface hydrogenation theories. Observations of warm NH_3 in IRC+10216 have been used to derive fractional abundances of 0.2–2.0×10^{-6} (Keady & Ridgway 1993; Monnier et al. 2000; Hasegawa et al. 2006). We assume that the abundance of NH_3 at other metallicites will scale with the dust surface area. For the LMC and SMC, this quantity and the associated gas-to-dust ratio and grain-size distribution are *highly* uncertain, although work is currently ongoing to determine more definite values. Assuming that the grain-size distribution in LMC and SMC carbon stars is similar to that in Galactic carbon stars, and that the gas-to-dust ratio scales with metallicity, we will adopt the upper observed fractional abundance of NH_3 for Galactic carbon stars, and scale according to metallicity for the LMC and SMC carbon stars. We apply a similar reasoning for scaling the initial fractional abundances of CH_4 and SiH_4 with metallicity.

Adopting the initial abundances detailed in Table 1 means that only small amounts of nitrogen, oxygen and sulphur are available for incorporation into other molecules and dust. However, in the Galactic case, some 5 per cent of the elemental carbon remains for incorporation into molecules or carbonaceous dust. At LMC and SMC metallicities, the percentage of free carbon rises to 28 per cent and 32 per cent, respectively, which is in reasonable agreement with Ferrarotti & Gail (2006) for an evolved star. These authors also found that at most 9 per cent of elemental silicon condensed into dust. Our initial abundances mean that 52–60 per cent of the elemental silicon is available for dust or dust seed formation.

In Table 2, we have compiled a comparison of C/O ratios and the carbon excesses ($\log(\epsilon_C - \epsilon_O)$) for the three metallicity regimes. C/O ratios increase drastically in the nucleosynthesis calculations of Karakas (2010), largely due to the decrease in elemental oxygen. The carbon excess is larger at low metallicity, an effect which has been observed (e.g. Wahlin et al. 2006).

2.2 Mass-loss rate

Mass-loss rates for AGB stars are generally measured using observations of the CO envelope and then assuming a CO-to-H_2 scaling ratio (the so-called X-factor, X_{CO}). Alternatively, the near- and mid-infrared spectral energy distribution can be fitted with a radiative-transfer model to obtain a dust mass-loss rate, and then by assuming

Table 1. Initial model fractional abundances (w.r.t. H_2).

Species	Observed Galactic inner envelope abundance	TE abundance (Galactic)	Adopted initial abundance (Galactic)	Adopted initial abundance (LMC)	Adopted initial abundance (SMC)
CO	[a]6×10^{-4}	4.4×10^{-4}	4.4×10^{-4}	1.7×10^{-4}	8.9×10^{-5}
N_2	[b]$-$	5.4×10^{-5}	5.4×10^{-5}	1.2×10^{-5}	3.9×10^{-6}
C_2H_2	[c]8×10^{-5}	3.3×10^{-5}	3.3×10^{-5}	2.8×10^{-4}	3.1×10^{-4}
HCN	[d]2×10^{-5}	2.4×10^{-5}	2.4×10^{-5}	3.3×10^{-5}	2.0×10^{-5}
SiS	[e]3×10^{-6}	3.7×10^{-6}	6.9×10^{-6}	2.1×10^{-6}	1.0×10^{-6}
CS	[c]4×10^{-6}	4.7×10^{-6}	2.4×10^{-6}	1.6×10^{-6}	8.0×10^{-7}
NH_3	[f]2×10^{-6}	3.3×10^{-11}	2.0×10^{-6}	8.0×10^{-7}	4.0×10^{-7}
CH_4	[c]2×10^{-6}	6.1×10^{-9}	2.0×10^{-6}	8.0×10^{-7}	4.0×10^{-7}
SiO	[g]1×10^{-6}	2.0×10^{-8}	1.7×10^{-6}	6.8×10^{-7}	3.6×10^{-7}
SiH_4	[c]2×10^{-7}	8.8×10^{-15}	2.0×10^{-7}	8.0×10^{-8}	4.0×10^{-8}

[a]Kwan & Linke (1982). [b]Not observed due to lack of permanent dipole. 2×10^{-4} is usually assumed in models (e.g. Cordiner & Millar 2009) similar to the elemental abundance. [c]Keady & Ridgway (1993), Cernicharo et al. (1999). [d]Schöier et al. (2007a), Cernicharo et al. (1999). [e]Schöier et al. (2007b), Decin et al. (2010). [f]Hasegawa et al. (2006), Monnier et al. (2000), Keady & Ridgway (1993). [g]Schöier et al. (2006), Keady & Ridgway (1993).

Table 2. C/O ratios, elemental carbon and oxygen abundances (ϵ_C, ϵ_O), and carbon excesses in the three metallicity environments.

Environment	ϵ_C	ϵ_O	C/O	C$-$O
MW	9.05	8.94	1.3	2.5×10^{-4}
LMC	9.33	8.53	6.3	1.8×10^{-3}
SMC	9.33	8.25	12.0	2.0×10^{-3}

Table 3. Physical parameters of the fiducial models.

Parameter	MW	LMC	SMC
$\dot{M}$ ($M_\odot$ yr^{-1})	3×10^{-5}	3×10^{-5}	3×10^{-5}
$1/\Psi$	100	200	500
v_{exp} (km s^{-1})	20	10	5
G (G_0)	1	2	4

$\dot{M}$ is the mass-loss rate, Ψ the dust-to-gas ratio, v_{exp} the envelope expansion velocity and G the interstellar UV field.

a gas-to-dust ratio, the total (gas+dust) mass-loss rate can be calculated. The former method has been routinely used for Galactic stars, but extragalactic stars are in general too faint. The availability of high-sensitivity data from, for example, the *Infrared Space Observatory* or the *Spitzer Space Telescope*, means that the second method is more practicable for extragalactic sources, and a large number of authors have taken this approach – see for example van Loon et al. (1999b) or Groenewegen et al. (2009) and references therein for mass-loss derivations for stars in the LMC and SMC. However, these two methods probe different parts of the CSE (e.g. Kemper et al. 2003), and often give differing values of total mass-loss rate.

Mass-loss rates for AGB stars in the Galaxy range from 10^{-9} to 10^{-4} $M_\odot$ yr^{-1}, with the median being 3×10^{-7} $M_\odot$ yr^{-1} (Schöier & Olofsson 2001; Olofsson 2008b). A typical mass-loss rate for a carbon star with a rich circumstellar chemistry such as IRC+10216 is $\approx 10^{-5}$ $M_\odot$ yr^{-1} (e.g. Men'shchikov et al. 2001; Woods et al. 2003). There seems to be no differentiation in the mass-loss rate based on chemistry (M-, C- and S-stars) in the Galactic sample of Olofsson (2008b) (see Fig. 2). There is a weak dependence on metallicity for O-rich stars compared to C-rich stars, with the difference appearing to be due to the driving mechanism of the

wind (e.g. Höfner 2007), and the opacity of the dust grains within it (Woitke 2006).

In the halo of our galaxy, where the metallicity is lower than that in the plane, a sample of 16 carbon-rich AGB stars have mass-loss rates of $\sim 4 \times 10^{-6}$ $M_\odot$ yr^{-1}, to within a factor of 3 (Mauron 2008). Similar, although smaller, rates are estimated by Groenewegen, Oudmaijer & Ludwig (1997) for two of these halo stars. In the metal-rich – but still sub-solar – Sagittarius dwarf spheroidal galaxy, six carbon stars are detected by Lagadec et al. (2010), who estimate mass-loss rates of the order of 10^{-6} $M_\odot$ yr^{-1}.

In the LMC and SMC, carbon stars have mass-loss rates similar to those in the Galaxy. Tanabé et al. (1997) found that dusty carbon-rich LMC stars have mass-loss rates less than 10^{-5} $M_\odot$ yr^{-1}; Leisenring et al. (2008) found that the brightest Magellanic carbon stars which made up their (biased) sample have mass-loss rates in a narrow range around 10^{-6} $M_\odot$ yr^{-1}; van Loon et al. (2003) found a particularly high mass-loss-rate carbon star, LI-LMC 1813, which has a mass-loss rate of nearly 4×10^{-5} $M_\odot$ yr^{-1}. Since this star is in a cluster, the birth mass and metallicity could be determined, allowing for an estimate of the dust-to-gas ratio (see Section 2.3). Various carbon stars have been observed in the SMC (e.g. van Loon et al. 1999a; Matsuura et al. 2005; van Loon et al. 2008) and rates are found to be similar to those in the LMC (see also van Loon 2000, 2006).

Since in this work we are only considering carbon stars, for our fiducial models in all three metallicity regimes we will assume $\dot{M} = 3 \times 10^{-5}$ $M_\odot$ yr^{-1}. This is towards the high end of the observed range of mass-loss rates, but typical of stars where the strong infrared C_2H_2 features are seen most clearly, and of the well-known Galactic carbon star IRC+10216.

2.3 Gas-to-dust ratio

In the early 1990s, Habing, Tignon & Tielens (1994) postulated that the dust-to-gas ratio would depend on metallicity, and this was refined by van Loon (2000) who determined observationally that it had an approximately linear dependence. Dust production at low metallicity is limited by the availability of heavy metals (e.g. titanium) to form the condensation seeds for dust formation (van Loon et al. 2008).

There have been several attempts to determine gas-to-dust ratios in the diffuse interstellar medium (ISM) of the MCs from H I and infrared maps. At higher densities this becomes almost impossible.

Moreover, it is not clear how the gas-to-dust ratio in the diffuse ISM relates to that in circumstellar environments. In the ISM of the LMC, the dust-to-gas ratio is approximately a quarter that of the solar value, and this has been established for several decades (e.g. van Genderen 1970; Koornneef 1982; Clayton & Martin 1985) and confirmed more recently with the *Herschel* and *Spitzer* telescopes (e.g. Gordon et al. 2003; Meixner et al. 2010). In the SMC, the ISM dust-to-gas ratio is about a tenth that of solar (van den Bergh 1968; van Genderen 1970; Lequeux et al. 1982; Bouchet et al. 1985; Bot et al. 2004; Gordon et al. 2009). Polycyclic aromatic hydrocarbons behave differently, but are also depleted at low metallicity (Sandstrom et al. 2012).

In the CSEs of AGB stars, the dust-to-gas ratio is harder to determine, especially without a good measure of the gas mass. This ratio also depends on chemistry: in *oxygen-rich* envelopes the dependence is roughly linear (Marshall et al. 2004). In carbon-rich envelopes, there is some decline with metallicity, but possibly slightly shallower than linear (van Loon 2000). Estimates derived from molecular band strengths (e.g. Sloan et al. 2006) can be misleading (van Loon et al. 2008). In lieu of firm determinations, authors have assumed various values: van Loon et al. (2003) assume a gas-to-dust value of 300–500 for the carbon star LI-LMC 1813; Leisenring et al. (2008) assume 100 for the Galaxy, 200 for the LMC and 500 for the SMC. We adopt 100, 200 and 500, respectively, in line with the metallicity for the fiducial models.

2.4 Wind expansion velocity

The expansion velocity of a CSE, that is, the terminal velocity once the wind has undergone acceleration in and close to the dust formation zone, depends on the dust-to-gas ratio, which in turn depends on the metallicity. There is also a lesser reliance upon the luminosity of the star, such that $v_{\mathrm{exp}} \propto \Psi^{1/2} L^{1/4}$, where Ψ is the dust-to-gas ratio, and L the luminosity (Habing et al. 1994; Elitzur & Ivezić 2001; Marshall et al. 2004). Thus, expansion velocity is expected to be lower in the MCs for a given luminosity.

There is also a link between expansion velocity and the mass-loss mechanism, since pulsation-driven winds (which are associated with low mass-loss rates) show low expansion velocities. Stars experiencing a superwind, where the mass-loss driver is radiation pressure on dust grains, generally show larger expansion velocities (e.g. Winters et al. 2000).

In general, expansion velocities in the LMC have been measured to be fairly small compared to the Galaxy. For all chemistries, Galactic expansion velocities cover a wide range, from low (e.g. 1.5–22.5 km s^{-1}; Olofsson 2008b) to high (e.g. 4.3–35.4 km s^{-1}; Loup et al. 1993) and even higher velocities are expected theoretically (e.g. up to 60 km s^{-1}; Mattsson, Wahlin & Höfner 2010). For Galactic carbon stars undergoing a superwind mass-loss, typical expansion velocities range from 13 to 22 km s^{-1} (e.g. Woods et al. 2003). In the LMC, van Loon et al. (2003) derived $v_{\mathrm{exp}} = 9.5$ km s^{-1} from modelling the carbon star LI-LMC 1813. In a sample of *oxygen-rich* CSEs in the LMC, Marshall et al. (2004) measured the expansion velocity of a number of OH masers and obtained results mostly in the region of 8–17 km s^{-1}. Circumstellar OH masers are thought to trace the terminal velocity of the wind, rather than H$_2$O masers, for example, which trace the acceleration zone. Wood, Habing & McGregor (1998) suggested that stars with higher expansion velocities have higher metallicities. More recently, van Loon (2000), Marshall et al. (2004) and Schöier et al. (2007a) have suggested that expansion velocities increase with evolution on the AGB. Expansion velocities for stars in the SMC have not been

determined. It should be noted that gas velocities and dust velocities are not necessarily well coupled, and drift velocities can be substantial at low mass-loss rates (e.g. Jones 2001).

One can also look to the Galactic Halo as a low-metallicity environment. Expansion velocities have been determined for several Halo stars: Groenewegen et al. (1997) measured an expansion velocity of 3.2 km s^{-1} from a ^{12}CO $J = 2$–1 line, which is exceptionally low for a carbon star. This value was confirmed by Lagadec et al. (2010), who observed the ^{12}CO $J = 3$–2 line. They also calculated a low (dust) mass-loss rate for this object. Lagadec et al. (2010) observed two other carbon stars in the Halo, and determined expansion velocities of 6.5 and 8.5 km s^{-1}. Three other carbon-rich objects in their sample were thought to be in the Galactic Halo, but instead reside within the Galaxy's more metal-rich thick disc. Expansion velocities for these stars were measured as 11.5–16.5 km s^{-1}. Theoretical models of AGB outflows (Mattsson et al. 2008; Wachter et al. 2008) show that although low expansion velocities may seem to be related to lower metallicity, they are more closely related to a low carbon excess: less dust formation implies a less efficient acceleration of the circumstellar material.

For the purposes of our fiducial models, we have adopted $v_{\mathrm{exp}} = 20$, 10 and 5 km s^{-1} for the Galaxy, LMC and SMC, respectively.

2.5 UV radiation field

Bernard et al. (2008) were able to establish that the ISRF in the LMC is in general stronger than that in the MW. They find that it varies from $0.8 \, G_0$ in diffuse regions to $3.5 \, G_0$ in molecular regions, with an average value of $\sim 2 \, G_0$. We use this value in our modelling. Such a galactic variation in field strength is also seen in the Galaxy, where the strength at the inner molecular ring can be up to five times that in the solar neighbourhood (Paladini et al. 2007). For the SMC, recent work by Sandstrom et al. (2010, fig. 10) has shown that the ISRF has an average value of $\sim 4 \, G_0$, although it can be as high as 10–$30 \, G_0$ in regions of star formation.

2.6 Caveats

Although we are presenting here three fiducial, and exploratory, models, not intended to represent any particular source, it is worth noting sources of uncertainties in our models, and how they may affect chemistry and predicted line intensities. Many of the physical parameters above have mainly an effect on the radius at which UV photons will dominate the chemistry of the envelope. Decreasing the mass-loss rate, increasing the expansion velocity of the wind or ISRF strength, or decreasing the dust-to-gas ratio (i.e. reducing the dust content) will have the effect of allowing greater penetration for UV photons, meaning that the envelope chemistry transitions to a photochemistry (rather than an ion–molecule or neutral–neutral chemistry) closer to the star. In practice, this means that parent molecules are destroyed more effectively, daughter species are produced and then destroyed in a narrower shell, and the distribution of species becomes more condensed. Since abundant parent species are found in the more dense parts of the envelope, where column densities are high, any changes to this threshold radius will have a minimal effect on the emission intensity from parents.

3 CHEMICAL MODELLING

Our chemical network is based on that of Cordiner & Millar (2009), augmented with silicon chemistry from the UMIST Database for

Astrochemistry 2006 (UDfA; Woodall et al. 2007). Reactions with Si-bearing species are included only for those species already present in the network of Cordiner & Millar (2009). The resulting network contains 481 chemical species, including atoms, neutral molecules, cations and anions, linked by 6174 reactions, which is considerably larger than the most recent release of UDfA, Rate06. Species range in size from single atoms (H, He, C, Mg, N, O, S, Si) to long hydrocarbon chains (e.g. C_{23}, $C_{23}H_2$).

We follow a parcel of gas as it passes from the inner edge of the CSE outwards at the terminal wind velocity. Since we assume a constant mass-loss process, this procedure is time independent, and we obtain a snapshot of the chemical structure of the CSE during the AGB phase. Chemical rate equations are solved using the Gear method for stiff differential equations (Gear 1971), resulting in fractional abundances for all species at each radial gridpoint.

4 RESULTS

Radial abundance profiles for various species are plotted in Figs 2–6, and we discuss different families of molecules as follows.

4.1 Carbon monoxide, polyynes and cyanopolyynes

Carbon monoxide (CO) in Galactic carbon stars is the most abundant molecule after H_2, and the most readily observable in the sub-

millimetre regime, given its high abundance and significant dipole moment. However, it is clear from the calculations that at lower metallicity (even at just half solar metallicity in the LMC), acetylene (C_2H_2) becomes the dominant carbon-bearing molecule for $R \lesssim 10^{16}$ cm (Fig. 2). In terms of column density through the envelope, $N(C_2H_2) \gtrsim N(CO)$ for LMC metallicity and is three times greater at SMC metallicity. The CO abundance is lower in LMC and SMC carbon stars, and this reduces the efficiency of self-shielding, meaning that the extent of the CO envelope is smaller in comparison.

The predominance of acetylene at lower metallicity means that the hydrocarbon chemistry is also more developed in such environments (Fig. 3). Acetylene and the ethynyl (C_2H) radical are the basis of much of the carbon-chain growth that occurs in carbon-rich circumstellar environments (Millar et al. 2000), and so larger species such as triacetylene (C_6H_2) experience a large boost in production. In the LMC and SMC models, $N(C_6H_2) = 3.5–3.9 \times 10^{17}$ cm^{-2}, whereas in the Galactic model the column density is 30 times smaller. The peak abundance of $C_{23}H_2$, the largest polyyne in the model, is comparable for the two lower metallicity regimes, but ~100 times smaller for the Galactic model. This increase in large hydrocarbons also applies to the cyanopolyyne chains (HC_3N, HC_5N, etc.) despite the reduction in elemental nitrogen abundance (Fig. 4). This would indicate that as metallicity decreases, nitrogen is preferentially sequestered in HCN and the cyanopolyynes rather than in other nitrogen-bearing species. Table 4, which gives an overview of the nitrogen repositories in the model by comparing column densities through the envelope, shows that this is the case. The abundance of HC_xN (odd $x \geq 3$) species increases from Galactic metallicity to LMC metallicity but decreases at SMC metallicities, following the changes in initial fractional abundance of HCN (Table 1).

The distribution of the cyanopolyyne chains is very different to that seen in Millar et al. (2000, fig. 6); however, it matches very well with the smooth density distribution model of Cordiner & Millar (2009). The difference arises from the inclusion of an increased photodissociation rate for HC_3N, resulting in a substantial reduction of the HC_3N/HC_5N ratio.

4.2 Anions

Several anions have now been detected in the Galactic carbon star IRC+10216: C_6H^- was identified by McCarthy et al. (2006), and confirmed by Cernicharo et al. (2007), who also reported the initial
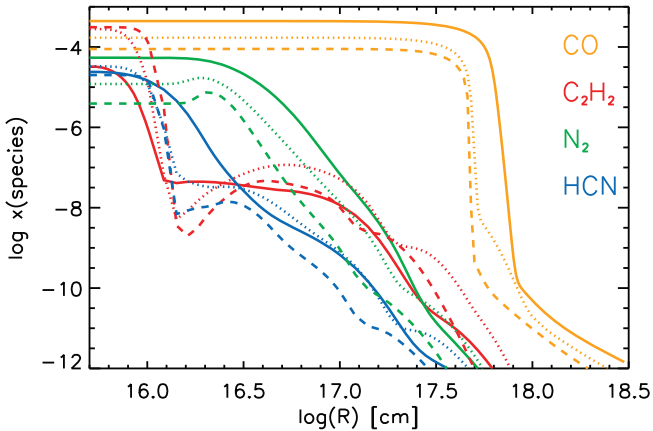

Figure 2. Fractional abundances of TE parent species. The solid line indicates the Galactic model, the dotted line indicates the LMC model and the dashed line indicates the the SMC model.
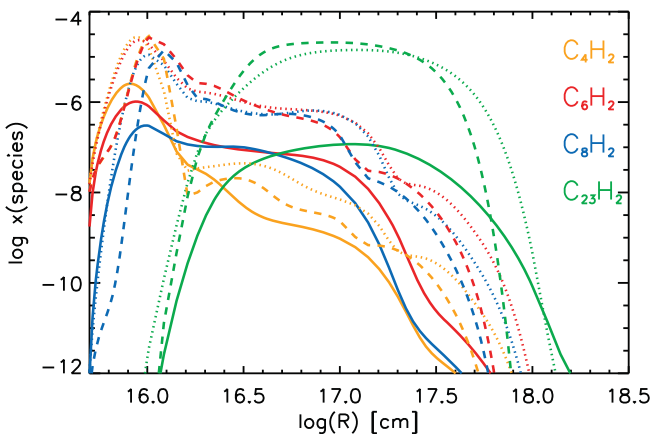

Figure 3. Fractional abundances of the polyyne species. Line characteristics are as in Fig. 2.
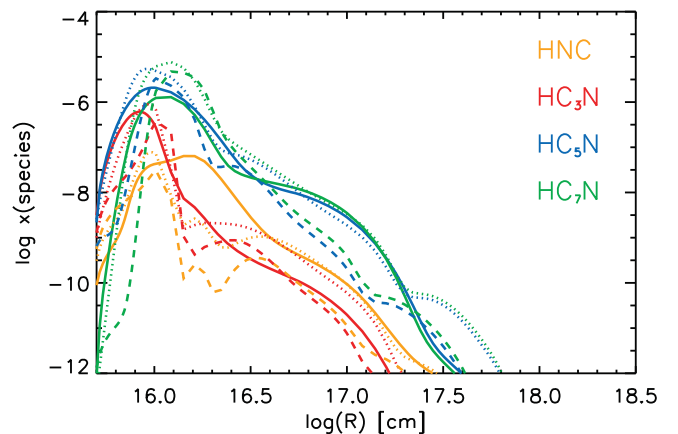

Figure 4. Fractional abundances of HNC and cyanopolyyne species. Line characteristics are as in Fig. 2.
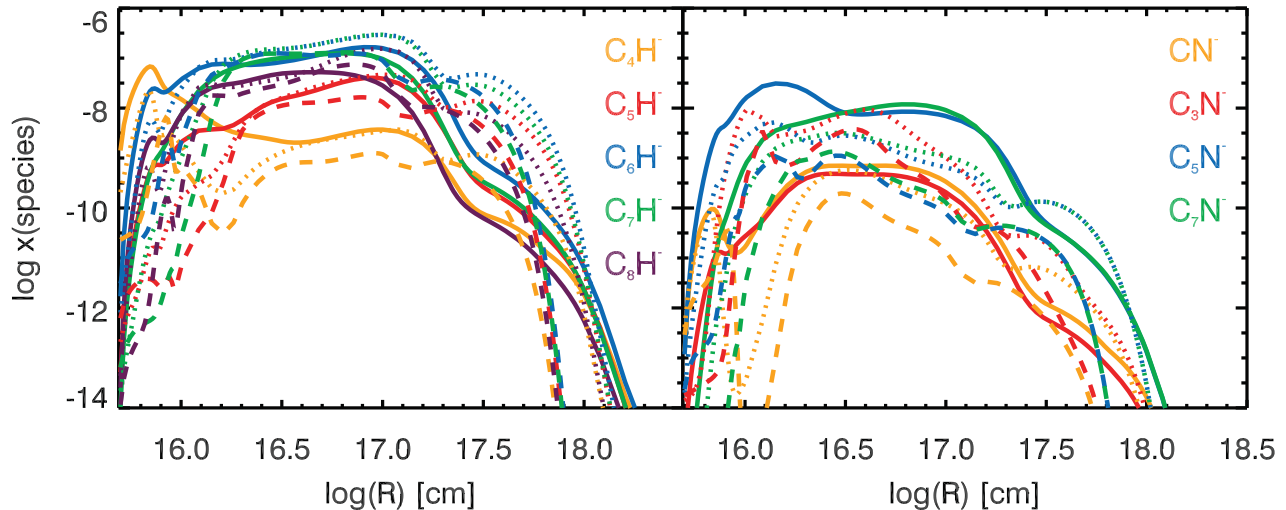
Figure 5. Fractional abundances of the anion species. Line characteristics are as in Fig. 2.
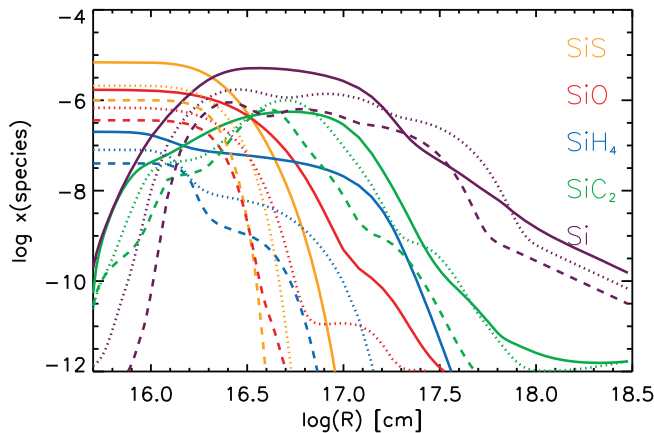

Figure 6. Fractional abundances of the silicon-bearing species. Line characteristics are as in Fig. 2.

detection of C_4H^-. C_8H^- was detected by Remijan et al. (2007) and Kawaguchi et al. (2007). The anions of the cyanopolyyne radicals C_3N and C_5N were discovered by Thaddeus et al. (2008) and Cernicharo et al. (2008), respectively. Most recently, Agúndez et al. (2010) detected the smallest molecular anion to date, CN^-. A summary of observed column densities and estimates of neutral-to-anion ratios is shown in Table 5. The anion chemistry is discussed in detail by Cordiner & Millar (2009).

In general, the radiative electron attachment rate of these carbon chains increases with length (Herbst & Osamura 2008); however, the abundance of the neutrals from which the anions are created

Table 4. Main nitrogen repositories at differing metallicities.

Species	MW (per cent)	LMC (per cent)	SMC (per cent)
N_2	71	37	25
HCN	14	42	58
N	12	12	12
$HC_{\Sigma(3...11)}N$	1	6	3
NH_3	1	1	1
CN	<1	<1	<1

peaks with C_6H, and hence the most abundant anions in these models are C_6H^- and C_7H^- (Fig. 5). We can compare the observed column densities and ratios for these anions with those calculated in our Galactic model (also shown in Table 5). Despite not specifically modelling IRC+10216, the agreement between model and observation is reasonably good for the smaller hydrocarbons. For column densities of the larger hydrocarbon anions, C_4H^- and larger, the agreement is not as close, with the model overproducing by factors of 100–1000. The abundances of these hydrocarbon anions are particularly sensitive to the initial abundance of acetylene, as has been discussed by Remijan et al. (2007). They show that a reduction in the initial abundance of acetylene by a factor of 5–10 brings about a much better overall agreement. The C_2H^- anion has not yet been detected, and we predict a column density of $\sim 10^9\,cm^{-2}$, several orders of magnitude below that of the detected anions. Thus, unless we have underestimated the radiative electron attachment rate of C_2H, C_2H^- is not likely to be detectable. Agúndez et al. (2010) have determined an upper limit for this species in IRC+10216, of <0.0014 per cent of the C_2H column (Table 5). Similarly, $C_{10}H^-$ has not been detected, but has a similar ion–neutral ratio to C_6H^- and C_8H^-, and a column density which is about a quarter of that of C_8H^-, according to the model. Also abundant in the envelope are negatively charged carbon chains, $C_{4...9}^-$, which have column densities of 8×10^{13}–$1 \times 10^{15}\,cm^{-2}$.

The distribution of hydrocarbon anions (Fig. 5) is similar for all members of the family from C_4H^- to C_8H^-. Similar distributions are also found for $C_{1,3,5,7}N^-$. At the inner peak of its distribution, at $\log(R) = 15.85$, CN^- is formed via electron attachment to MgNC, even in the lowest metallicity case. Agúndez et al. (2010) found that $HCN + H^- \longrightarrow CN^- + H_2$ provides a minor contribution in this region, but we find this reaction ineffective. The much broader, outer peak of the CN^- distribution arises due to the reaction $N + C_{4...7}^- \longrightarrow CN^- + C_{3...6}$. In general, the larger members of the family are all formed by electron attachment to corresponding neutrals. The distribution of CN^- fits well with the observations of Agúndez et al. (2010), and the column density calculated in the model ($3.0 \times 10^{12}\,cm^{-2}$) matches the observed determination ($8.0 \times 10^{12}\,cm^{-2}$) very closely. Similarly, the column density of C_3N^- ($1.6 \times 10^{12}\,cm^{-2}$) matches that determined for IRC+10216 by Thaddeus et al. (2008) exactly. Cernicharo et al. (2008) derived a rather low column density for C_5N^- of $3.4 \times 10^{12}\,cm^{-2}$ (lower than

Table 5. Column densities and ion–neutral ratios for anionic species in IRC+10216.

Species	Observed column density (cm^{-2})	Neutral–ion ratio	Reference	Calculated column density (cm^{-2})	Calculated neutral–ion ratio
CN$^-$	8.0×10^{12}	400	Agúndez et al. (2010)	3.0×10^{12}	~8 000
C$_3$N$^-$	1.6×10^{12}	200	Thaddeus et al. (2008)	1.6×10^{12}	~240
C$_5$N$^-$	3.4×10^{12}	2	Cernicharo et al. (2008)	1.3×10^{14}	6
C$_2$H$^-$	$<7 \times 10^{10}$	>70 000	Agúndez et al. (2010)	8.1×10^8	~10^8
C$_4$H$^-$	7.1×10^{11}	4 200	Cernicharo et al. (2007)	7.2×10^{14}	17
C$_6$H$^-$	4.0×10^{12}	16–100	McCarthy et al. (2006); Cernicharo et al. (2007)	8.2×10^{14}	4
C$_8$H$^-$	2.4×10^{12}	3–4	Remijan et al. (2007); Kawaguchi et al. (2007)	2.1×10^{14}	5

for CN$^-$), but note that this figure is likely to be an underestimate. We calculate a column density of $N(\mathrm{C_5N^-}) = 1.3 \times 10^{14}$ cm^{-2}.

At lower metallicity, small anions are a factor of a few lower in abundance than at Galactic metallicity. This is surprising given that the corresponding neutrals are more abundant, and the number of free electrons in the Magellanic envelopes is larger. The larger anions C$_6$H$^-$ and C$_7$H$^-$ are predicted to be more abundant at LMC metallicity than Galactic.
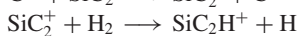
4.3 Silicon chemistry

Silicon chemistry was not included in the model of Cordiner & Millar (2009), but is included here due to the potentially important reaction

$$\mathrm{C_2H_2 + Si \longrightarrow SiC_2 + H_2,} \qquad (2)$$

which could be a major sink of C$_2$H$_2$ in the inner regions of the envelope at low metallicity. However, the model shows that reactions with other hydrocarbons are the major loss mechanisms for C$_2$H$_2$, even in the highest metallicity case (i.e. where the abundance of silicon atoms is highest).

SiC$_2$ was recently detected by the *Herschel Space Observatory* in IRC+10216 (Cernicharo et al. 2010), where its distribution traces the dust-formation zone of the star, similar to SiO and SiS emission (Fonfría et al. 2008). However, it also has a significant abundance in the outer envelope (Gensheimer, Likkel & Snyder 1995; Lucas et al. 1995), as we find in our modelling (see Fig. 6), with the distribution peaking at ~5×10^{16} cm and reaching $x(\mathrm{SiC_2}) = 5 \times 10^{-7}$. These figures correspond well with the observations of Lucas et al. (1995) and the chemical model of Cernicharo et al. (2010). The abundance of SiC$_2$ increases through the reaction between acetylene and silicon atoms (equation 2), and it becomes destroyed outside $R = 10^{17}$ cm by reaction with abundant C$^+$ ions. The peak abundance of SiC$_2$ is similar in all metallicity regimes, and column densities are slightly enhanced in the LMC and SMC models (1.9×10^{15}:4.2×10^{15}:2.6×10^{15}; MW:LMC:SMC). The chemistry is slightly different in the LMC and SMC models, since the neutralization of SiC$_2$H$^+$ to form SiC$_2$ dominates over reaction (2). SiC$_2$H$^+$ itself is partially formed from SiC$_2$, via the chain

$$\mathrm{Si^+ + C_2H \longrightarrow SiC_2^+ + H}$$
$$\mathrm{C^+ + SiC_2 \longrightarrow SiC_2^+ + C}$$
$$\mathrm{SiC_2^+ + H_2 \longrightarrow SiC_2H^+ + H}$$
$$\mathrm{SiC_2H^+ + e^- (or\ anion) \longrightarrow SiC_2 + H\ (+\ neutral).}$$

The major repository for silicon in CSEs is SiS (Table 6), in line with the high initial abundances of this molecule (Table 1). This is true in all metallicity regimes tested, although the abundance of SiS drops slightly with metallicity as sulphur is preferentially incorporated into CS.

Table 6. Main silicon repositories at differing metallicities.

Species	MW (per cent)	LMC (per cent)	SMC (per cent)
SiS	70	65	64
SiO	17	21	23
Si	6	6	5
Si$^+$	6	4	6
SiH$_4$	2	2	2
SiC$_2$	<1	2	2

4.4 The effect of assumptions about physical parameters

In order to fully understand the chemistry at low metallicity distinct from the effect of the differing physical conditions, we calculated three models adopting the physical conditions of the Galactic model (Table 3), and using the initial chemical abundances of the three different metallicity regimes. Hence, any variation in abundance or column density is solely due to the chemistry of the CSE, or the initial abundances adopted. For clarity, we will name these the 'fixed physics' models, as opposed to the 'full physics' models, as described previously.

In Table 7, we present the column densities derived from the full physics models, and their ratios. In the final column, we have listed the ratio of column densities derived from the fixed physics models. Looking at how the two final columns in the table change gives us an indication of how the adopted physical conditions affect the chemistry of the model.

For many of the species, metallicity is the dominating factor, with column densities falling with metallicity despite an increase in the overall H$_2$ column density. Many of the nitrogen-bearing species are included in this group, which makes them good tracers of metallicity: CN, CH$_3$CN, C$_5$N$^-$. However, there are exceptions to this: C$_3$N, C$_5$N, C$_3$N$^-$ and the cyanopolyynes increase in relative column density at LMC metallicity, but decrease at SMC metallicity. Species containing heavy metals such as silicon or magnesium also reflect changes in metallicity, with the exception to this being SiC$_2$. For SiC$_2$, the effect of the lowering metallicity is to produce a decrease in the column density (see the final column of Table 7). However, column densities in the full physics models increase for LMC and SMC metallicities, counteracting the effects due to chemistry alone. Another species with similar properties is CS, which is produced inherently less in lower metallicity environments, but receives a boost in production in the denser environments of the full physics models.

CO is not a very good tracer of metallicity in carbon stars, despite it being a good tracer of oxygen abundance under the fixed physics conditions. Observationally, CO emission is often optically thick,

Table 7. Calculated column densities (cm^{-2}) for species of interest.

Species	N_{MW}	N_{LMC}	N_{SMC}	Ratio	Ratio$_{physics}^{fixed}$
H$_2$	2.88×10^{22}	5.77×10^{22}	1.15×10^{23}	1.00: 2.00: 4.00	1.00: 1.00: 1.00
C$_2$H	7.88×10^{16}	7.33×10^{16}	2.64×10^{16}	1.00: 0.93: 0.33	1.00: 1.71: 1.78
C$_2$H$^-$	8.12×10^{8}	7.48×10^{8}	1.10×10^{9}	1.00: 0.92: 1.36	1.00: 0.94: 1.02
C$_2$H$_2$	5.28×10^{17}	1.06×10^{19}	2.89×10^{19}	1.00:20.08:54.77	1.00: 7.95: 8.76
C$_2$S	2.67×10^{14}	3.43×10^{14}	1.78×10^{14}	1.00: 1.28: 0.67	1.00: 0.99: 0.50
CH$_3$CN	1.65×10^{13}	1.88×10^{12}	2.81×10^{12}	1.00: 0.11: 0.17	1.00: 0.18: 0.07
CN	2.46×10^{16}	1.48×10^{16}	8.84×10^{15}	1.00: 0.60: 0.36	1.00: 0.62: 0.35
CN$^-$	3.01×10^{12}	2.93×10^{12}	1.46×10^{12}	1.00: 0.97: 0.48	1.00: 0.92: 0.47
CO	1.29×10^{19}	9.93×10^{18}	1.04×10^{19}	1.00: 0.77: 0.81	1.00: 0.39: 0.20
CS	5.66×10^{16}	7.67×10^{16}	8.01×10^{16}	1.00: 1.36: 1.42	1.00: 0.65: 0.32
C$_3$H	5.92×10^{14}	1.04×10^{15}	6.29×10^{14}	1.00: 1.75: 1.06	1.00: 2.01: 1.81
C$_3$H$_2$	3.03×10^{14}	7.37×10^{14}	8.19×10^{14}	1.00: 2.43: 2.70	1.00: 2.80: 2.53
C$_3$N	3.92×10^{14}	6.08×10^{14}	1.87×10^{14}	1.00: 1.55: 0.48	1.00: 1.63: 0.95
C$_3$N$^-$	1.64×10^{12}	1.77×10^{12}	7.93×10^{11}	1.00: 1.08: 0.48	1.00: 1.13: 0.60
C$_3$S	1.03×10^{15}	1.47×10^{15}	5.87×10^{14}	1.00: 1.43: 0.57	1.00: 1.20: 0.62
C$_4$H	1.21×10^{16}	2.00×10^{16}	6.57×10^{15}	1.00: 1.65: 0.54	1.00: 3.30: 3.86
C$_4$H$^-$	7.18×10^{14}	3.04×10^{14}	1.11×10^{14}	1.00: 0.42: 0.15	1.00: 0.99: 0.93
C$_4$H$_2$	2.89×10^{16}	4.35×10^{17}	3.55×10^{17}	1.00:15.04:12.26	1.00:11.63:12.85
C$_5$N	7.51×10^{14}	1.84×10^{15}	6.28×10^{14}	1.00: 2.45: 0.84	1.00: 2.79: 1.80
C$_5$N$^-$	1.33×10^{14}	4.10×10^{13}	9.11×10^{12}	1.00: 0.31: 0.07	1.00: 0.52: 0.29
C$_6$H$^-$	8.24×10^{14}	1.84×10^{15}	1.73×10^{15}	1.00: 2.23: 2.09	1.00: 2.16: 2.31
C$_6$H$_2$	1.15×10^{16}	3.86×10^{17}	3.51×10^{17}	1.00:33.55:30.50	1.00:24.63:29.99
C$_8$H$^-$	2.14×10^{14}	7.35×10^{14}	8.22×10^{14}	1.00: 3.44: 3.85	1.00: 2.07: 2.13
HCN	5.45×10^{17}	1.44×10^{18}	1.94×10^{18}	1.00: 2.64: 3.55	1.00: 1.20: 0.71
HC$_3$N	6.44×10^{15}	1.27×10^{16}	5.26×10^{15}	1.00: 1.97: 0.82	1.00: 1.74: 1.02
HC$_5$N	1.89×10^{16}	8.66×10^{16}	3.97×10^{16}	1.00: 4.58: 2.09	1.00: 3.59: 2.31
HNC	2.95×10^{14}	9.11×10^{14}	7.46×10^{14}	1.00: 3.08: 2.53	1.00: 4.77: 3.62
MgNC	3.92×10^{15}	3.01×10^{15}	1.81×10^{15}	1.00: 0.77: 0.46	1.00: 0.39: 0.15
SiC	1.10×10^{14}	5.22×10^{13}	3.02×10^{13}	1.00: 0.48: 0.27	1.00: 0.43: 0.24
SiC$_2$	1.93×10^{15}	4.17×10^{15}	2.56×10^{15}	1.00: 2.16: 1.33	1.00: 0.92: 0.47
SiN	1.05×10^{14}	2.48×10^{13}	1.19×10^{13}	1.00: 0.24: 0.11	1.00: 0.15: 0.04
SiO	4.37×10^{16}	3.49×10^{16}	3.70×10^{16}	1.00: 0.80: 0.85	1.00: 0.40: 0.21
SiS	1.77×10^{17}	1.08×10^{17}	1.03×10^{17}	1.00: 0.61: 0.58	1.00: 0.31: 0.15

List of molecules observed by He et al. (2008) in IRC+10216, with the addition of those in bold face.

and thus the observed flux intensity is not representative of the abundance of CO. In addition, in our models, column densities of CO in the full LMC and SMC models are comparable, despite a factor of 2 difference in metallicity. CO is a very good tracer of the molecular envelope of carbon stars, though, and gives us an indication (see Fig. 2) that in general, the envelopes of Magellanic carbon stars will only extend ~70 per cent of the distance of similar Galactic carbon stars.

The column densities of hydrocarbons such as C$_2$H$_2$, C$_4$H, C$_4$H$_2$ and C$_6$H$_2$ increase significantly at lower metallicity, as we have seen. Table 7 shows that much of this increase is due to the changes in chemistry at lower metallicity, with the relative proportion of carbon increasing over oxygen (Table 2). A significant increase in column density for these species is also due to the differing physical conditions found in Magellanic carbon stars. These species are formed through neutral–neutral reactions, and the higher densities of Magellanic envelopes mean that these reactions proceed more quickly. This trait is not observed to the same degree in anions of hydrocarbon species, which are generally more abundant than in Galactic carbon stars for larger species (C$_6$H$^-$ and larger), but only by a factor of a few. This is somewhat surprising, since the ionization fraction of the envelope almost doubles from Galactic model to LMC model to SMC model. Smaller hydrocarbon species (C$_4$H$^-$, C$_5$H$^-$) are more abundant in Galactic CSEs.

5 OBSERVABLES

With the impending completion of ALMA in 2013, it is interesting to consider the potential for ALMA to observe molecular line emission from extragalactic AGB CSEs, focusing on the MCs. We have estimated line intensities for nearly half a million lines assuming local thermal equilibrium (LTE) (Section 5.1), and selected a few potential candidate lines for further investigation using a more rigorous non-LTE radiative transfer code (Section 5.2).

5.1 LTE estimates

Following the calculations of Olofsson (2008a), one can write

$$S_{CO(2-1)} \approx 6 \left[\frac{\dot{M}}{10^{-6}}\right]^{1.2} \left[\frac{15}{v_e}\right]^{1.6} \left[\frac{X_{CO}}{10^{-3}}\right]^{0.7} \left[\frac{1}{D}\right]^2 \text{ Jy}, \tag{3}$$

where the CO ($J = 2–1$) line flux density is given in terms of the mass-loss rate, expansion velocity, fraction of CO with respect to H$_2$ and the distance, D, to the star. Inserting typical values for the LMC gives us an estimated flux density of $\approx$0.04 Jy. Similarly, for the SMC, we calculate $S_{CO(2-1)} \approx 0.09$ Jy, since we expect the density of CSEs in the SMC to be higher. Comparable flux densities are expected for the CO ($J = 3–2$) line. Such stars should be easily detectable within an hour's observations for the full ALMA array ($5\sigma = 6$ mJy at 2 km s^{-1} resolution). Stars with properties similar to

Table 8. Predicted line strengths for carbon stars in the LMC, using equation (4).

Band 3 (89–119 GHz)			Band 6 (211–275 GHz)			Band 7 (275–370 GHz)		
Molecule	Frequency (GHz)	Peak flux (mJy)	Molecule	Frequency (GHz)	Peak flux (mJy)	Molecule	Frequency (GHz)	Peak flux (mJy)
C_4H_2	89.315	0.1	SiO	217.105	0.7	CS	293.912	0.3
C_4H_2	89.687	0.1	^{13}CO	220.399	1.0	SiO	303.927	0.3
SiC_2	93.064	0.1	CN	226.632	0.2	^{13}CO	330.588	1.7
C_4H_2	97.834	0.1	CN	226.660	0.6	CN	340.008	0.1
CS	97.981	0.1	CN	226.664	0.2	CN	340.020	0.1
C_4H_2	98.245	0.1	CN	226.679	0.2	CN	340.032	1.1
C_4H_2	98.655	0.1	CN	226.874	0.6	CN	340.035	0.4
C_4H_2	107.175	0.1	CN	226.875	0.9	CN	340.035	0.7
^{13}CO	110.201	0.1	CN	226.876	0.4	CN	340.248	1.0
CN	113.491	0.1	CN	226.887	0.1	CN	340.248	1.4
CO	115.271	2.5	CN	226.892	0.1	CN	340.249	0.8
SiC_2	115.382	0.2	CO	230.538	≈40	CS	342.883	0.1
C_4H_2	116.105	0.1	CS	244.936	0.5	CO	345.796	≈40
			SiO	260.518	0.5	SiO	347.331	0.1
			C_2H	262.004	1.5	C_2H	349.338	1.3
			C_2H	262.006	1.1	C_2H	349.339	1.0
			C_2H	262.065	1.1	C_2H	349.399	1.0
			C_2H	262.067	0.7	C_2H	349.401	0.8
			c-C_3H_2	265.759	0.1	HCN	354.505	58.9
			HCN	265.886	66.7	c-C_3H_2	368.294	0.4

Band 9 (602–720 GHz): strongest lines include $C_2H_3^+$, HCN and CO, all with intensities of the order of 1 mJy.

our LMC stellar characteristics should be detectable out to ≈150 kpc within 1 h, whilst stars similar to our SMC stellar characteristics could potentially be seen out to distances of ≈200 kpc within an hour (Olofsson 2008a).

For species other than CO, the line flux density can also be estimated (Olofsson 2008a). For LMC carbon stars,

$$S \approx 1.62 \times 10^{-9} g_u A_{ul} f_X R_e \frac{e^{-E_1/kT_X}}{Q(T_X)} \text{ Jy}, \tag{4}$$

using our standard parameters, and where g_u, A_{ul} and E_l are the quantum mechanical degeneracy of the upper energy level of the transition, the Einstein coefficient for the transition and the energy of the lower energy level, respectively. $Q(T_X)$ is the partition function, dependent on the excitation temperature of the molecule, T_X, which we assume to be 10 K for all rotational transitions (cf. Woods et al. 2003). R_e is the radius of the emitting region for each molecule, taken from the molecular distributions in the chemical model. Similarly for the SMC,

$$S \approx 3.72 \times 10^{-9} g_u A_{ul} f_X R_e \frac{e^{-E_1/kT_X}}{Q(T_X)} \text{ Jy}. \tag{5}$$

Estimated flux densities for molecular lines stronger than 0.1 mJy are given in Table 8. The peak line intensities calculated from equations (4) and (5) generally underestimate line strengths by a factor of ≈5–50 in comparison to those from the non-LTE model (Section 5.2). The exception to this is lines of HCN, which are overestimated by ≈9–16 times in comparison to the NLTE estimates. Our assumption of $T_X = 10$ K for HCN lines is probably a significant underestimate for a species which is only abundant in the inner regions of the CSE. Adopting $T_X = 75$ K reduces $S_{HCN(3-2)} \approx 27$ mJy, approximately halving the estimate for $T_X = 10$ K.

5.2 Non-LTE estimates

In addition to our simple estimates for the expected line flux density described above, we have used the one-dimensional non-LTE Monte

Carlo radiative transfer code, RATRAN (Hogerheijde & van der Tak 2000), to estimate the line profiles and line strengths of molecular line emission from evolved carbon stars in the LMC and SMC. In our simple estimates (see equations 4 and 5), we assume LTE and an excitation temperature of 10 K for all rotational transitions. In reality, the envelopes of AGB stars have a radially dependent temperature and density structure (see e.g. Jura & Morris 1981) which limits the accuracy of calculations made with these assumptions. The temperature varies from ~1000 K in the inner envelope to ~10 K in the outer envelope. Similarly, the density structure exhibits an R^{-2} behaviour so that in the outer envelope the density is much lower than the critical density of rotational transitions ($A_{ul}/\Sigma_i C_{ui}$, where i indicates all energy levels lower than the upper level, u). We used molecular data from the Leiden Atomic and Molecular Database (LAMDA[2]) which has tabulated energy levels, Einstein A coefficients and collisional rates for many molecules with transitions in the (sub-)mm region of the electromagnetic spectrum (Schöier et al. 2005).

In our radiative transfer calculations, as in the physical and chemical modelling, we treat the stellar envelope as spherically symmetric with a constant outward stellar wind velocity of 10 km s^{-1} for the LMC and 5 km s^{-1} for the SMC. Since our line profiles are broadened to a width ≳20 and ≳10 km s^{-1}, respectively, we use a spectral resolution of 1 km s^{-1} for both sources. We assume a distance to source of 50 kpc for the LMC and 66 kpc for the SMC. We generated line profiles and line strengths for rotational transitions of CO, CS, CN, HCN, SiO and SiS which fall into the expected spectral range of ALMA 'Full Science' operations (≈30 to ≈950 GHz). These are the molecules which our calculations suggested may be sufficiently abundant to possess emission strong enough to be observable and for which collisional rates are available. Using the ALMA sensitivity calculator,[3] we determined those line transitions which may be

Table 9. Estimated observation times for ALMA Full Science, using the ALMA Sensitivity Calculator.

Molecule	Transition (J)	Frequency (GHz)	LMC Peak flux (mJy)	S/N	Integration time	SMC Peak flux (mJy)	S/N	Integration time
CO	1–0	115.271	19.2	10	50.4 min	19.8	10	47.2 min
	2–1	230.528	64.2	10	1.3 min	65.3	10	1.3 min
	3–2	345.796	69.0	10	2.8 min	67.5	10	3.0 min
	4–3	461.041	65.4	10	2.6 h	57.8	10	3.9 h
	6–5	691.473	64.2	5	1.4 h	52.9	5	2.5 h
HCN	3–2	265.886	4.1	5	1.6 h	2.6	5	4.2 h
	4–3	354.505	6.7	5	1.7 h	4.2	5	4.5 h
CS	5–4	244.936	2.8	5	2.6 h	2.7	5	2.6 h
	6–5	293.912	3.8	5	2.1 h	3.5	5	2.8 h
	7–6	342.883	4.7	5	2.7 h	4.3	5	2.8 h
SiO	5–4	217.105	3.9	5	1.4 h	2.7	5	3.6 h
	6–5	260.518	5.0	5	1.0 h	3.6	5	2.0 h
	7–6	303.927	5.9	5	1.0 h	4.3	5	1.8 h
	8–7	347.331	6.4	5	1.3 h	4.8	5	2.4 h
SiS	12–11	217.817	2.9	5	2.5 h	2.7	5	3.6 h
	13–12	235.961	3.1	5	2.7 h	3.0	5	2.8 h
	14–13	254.103	3.3	5	2.0 h	3.3	5	2.0 h
	15–14	272.243	3.4	5	2.1 h	3.5	5	2.2 h
	16–15	290.380	3.5	5	2.6 h	3.6	5	2.7 h
	17–16	308.516	3.5	5	3.2 h	3.7	5	3.3 h
CN	2–1	226.333	2.3	5	3.6 h	1.9	5	5.7 h
	2–1	226.659	6.0	5	37.6 min	4.4	5	1.1 h
	3–2	340.031	4.4	5	2.7 h	3.7	5	4.6 h
	3–2	340.249	9.1	5	39.9 min	6.9	5	1.1 h

In our integration time estimates, we assume an array size of 50 antennas and a spectral resolution of $2.0\,\mathrm{km\,s^{-1}}$.
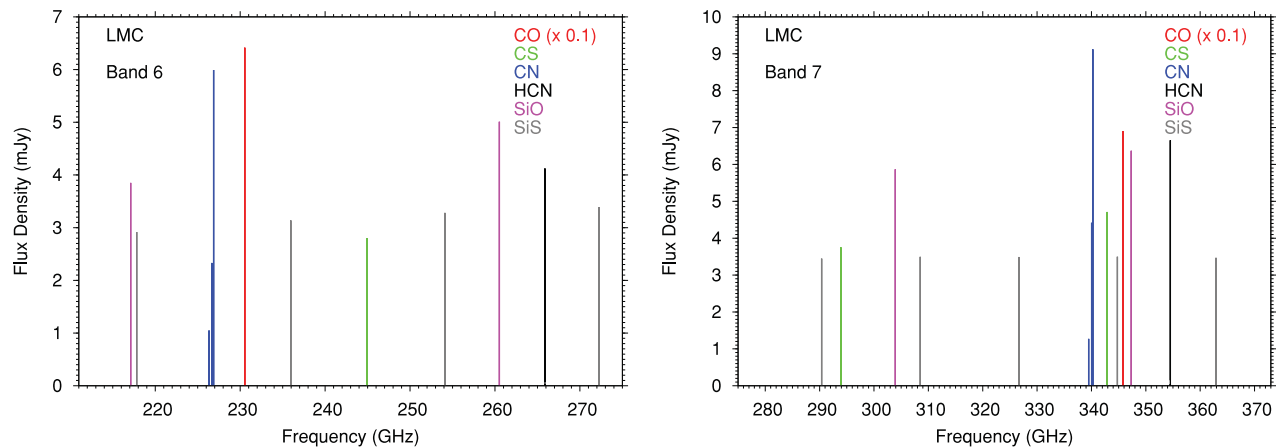
Figure 7. Synthetic spectra of an LMC carbon star for ALMA Bands 6 and 7.

observable with ALMA Full Science within a realistic observing time. Our results are listed in Table 9. We determine that molecular transitions in Bands 6 and 7 make particularly good targets. Assuming a spectral resolution of $2\,\mathrm{km\,s^{-1}}$ and an array size of 50 antennas, we find the observation times for LMC and SMC molecular transitions range from a few minutes for the CO $J = 2$–1 and $J = 3$–2 transitions at 230 and 345 GHz to several hours for transitions of HCN, CS, SiO, SiS and CN which also fall into Bands 6 and 7. In addition, the CO $J = 1$–0 transition, in Band 3, may also be observable to high signal-to-noise ratio within 1 h in evolved stars within both galaxies. We note here that our time calculations are likely upper estimates since the ALMA full array may eventually consist of up to 66 antennas in total. Also the online ALMA sensitivity calculator overestimates the predicted observing times relative to

the more accurate calculator available using the ALMA Observing Tool, again, indicating that our predicted times are likely upper estimates. In Figs 7 and 8, we present the expected line spectra due to emission from the listed molecules from a carbon star in both the LMC and SMC, for ALMA Bands 6 and 7. Line profiles of each line transition are also provided as Supporting Information with the online version of the paper (Figs 9–32). Reducing the mass-loss rate of the models by a factor of 3 reduces the line strengths in Table 9 by a similar factor. Thus, probing the molecular inventory of carbon stars with low mass-loss rates in the MCs will be challenging.

Looking first at the predicted line spectra for the LMC (Fig. 7), we see that the strongest transitions are due to CO, CN, HCN and SiO. Multiple transitions of CN, SiO, CS and SiS are available within a single band which would allow determination of the
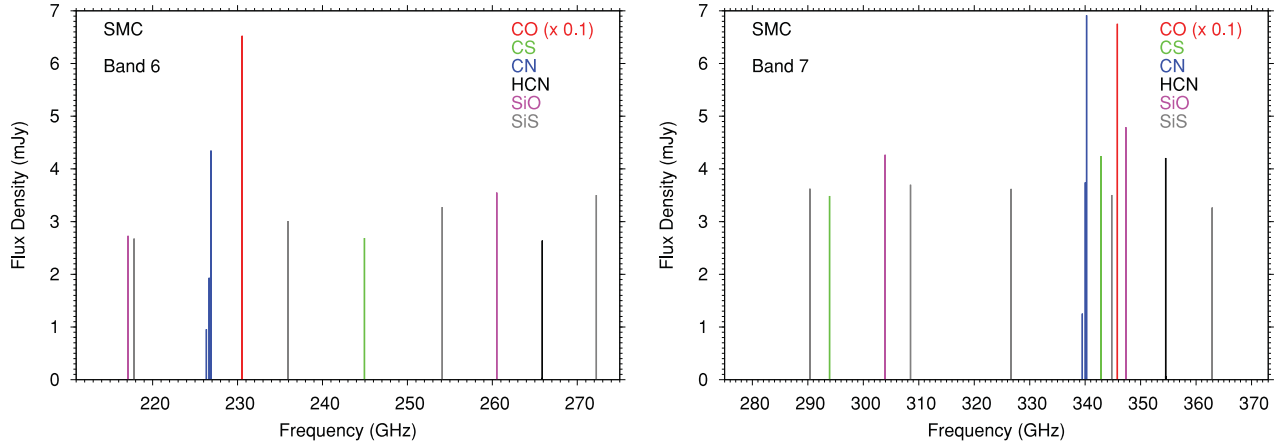
Figure 8. Synthetic spectra of an SMC carbon star for ALMA Bands 6 and 7.

temperature and density of the emitting gas, enabling some constraints on the physical conditions in the envelope. For the SMC (Fig. 8), we see a similar pattern; however, we now find that transitions of SiS are comparable in strength with those of SiO and HCN. Comparing the two metallicity regimes, we see differences in the line strength ratios between CO/CN and SiO/SiS, with these ratios generally decreasing with metallicity. This follows, given the decreased amount of oxygen available in the SMC relative to the LMC. We also see that the line strength ratios of CN/HCN slightly increase with metallicity, likely related to the increased strength of the ISRF in the SMC. Our calculations demonstrate that there are observable tracers of metallicity and physical conditions in extragalactic carbon stars which ALMA will allow us to probe.

6 DISCUSSION

This investigation was prompted by the observation of very common and very deep molecular absorptions due to C_2H_2 in the mid-infrared spectra (5–38 µm) of LMC carbon stars (e.g. Woods et al. 2011, for a number of examples) compared to Galactic carbon stars. This occurs particularly in the extreme carbon stars, which are losing mass at very high rates. Of course, the fact that these deep features exist has been established for several years: Speck et al. (2006) analysed the deepest C_2H_2 absorption feature observed to date; Zijlstra et al. (2006) noted that acetylene bands were stronger at low metallicity; Leisenring et al. (2008) measured equivalent widths of molecular lines; Sloan et al. (2006) and Lagadec et al. (2007) detected acetylene absorptions in SMC carbon stars that appeared deeper than in corresponding Galactic and LMC carbon stars. There have also been studies in the acetylene-dominated 3.1/3.8 µm bands which show similar results (van Loon et al. 1999a; Matsuura et al. 2002, 2005; van Loon 2006). van Loon et al. (2008) performed a 3 µm band study, finding that acetylene absorption features in LMC and SMC carbon stars were equivalent in depth. The origin of the 3 µm acetylene band is a mixture of photospheric and circumstellar origin (van Loon 2006), whereas the 13.7 µm absorption seen in *Spitzer* spectra is predominantly circumstellar (Matsuura et al. 2006). We have shown via TE calculations that 'photospheric' acetylene increases in abundance as the metallicity is lowered (Fig. 1), qualitatively matching what we observe at 3 µm. We have also shown via radially dependent non-equilibrium calculations that indeed acetylene is more abundant in carbon-rich CSEs at lower metallicity (Fig. 2). Initial investigations into carbon stars in other low(er) metallicity galaxies show that acetylene features are

also very strong (e.g. Sloan et al. 2009). Unfortunately we do not yet have sufficiently good quality infrared data to perform quantitative analyses.

Related to the study of acetylene is the study of hydrogen cyanide. It absorbs in the 3.1 µm band with acetylene, and also forms part of the 13.7 µm band, absorbing at ∼14 µm. There is also a band at 7 µm, close to the acetylene band at 7.5 µm. Its contribution to these bands has been detected in a number of Magellanic carbon stars, but not nearly so prevalently as acetylene (e.g. Matsuura et al. 2005; Zijlstra et al. 2006; van Loon 2006). In some objects, the absorptions are strong (Matsuura et al. 2002), whereas in other objects, absorptions are very weak (Matsuura et al. 2008). Both the TE model and the CSE model predict high abundances of HCN at low metallicity, despite the lower abundance of elemental nitrogen. This would imply that both the 3 and 13.7 µm bands should show ample evidence of HCN absorption. Our high abundances may be an effect of our choice of $3\,M_\odot$ nucleosynthesis models (Section 2.1) since the nitrogen abundance in AGB stars is dependent on (initial) stellar mass, such that stars with high luminosity (i.e. high initial mass) should have abundant HCN (Matsuura et al. 2005). The variation in feature strength seen in the infrared may reflect varying initial stellar mass in the observed samples. The impact of different choices of stellar mass should be looked into in future models. Scaling initial abundances up or down uniformly generally results in a similar scaling of CSE abundances; however, changes in stellar mass are unlikely to produce such a uniform scaling, but would result in abundance enhancements in some elements over others.

Emission from two large circumstellar molecules was observed recently in Magellanic objects. The fullerenes C_{60} and C_{70} have been detected in a decade of planetary nebulae (PNe; García-Hernández et al. 2011; Zhang & Kwok 2011 provides a summary of all fullerene detections) in the LMC, as well as several Galactic objects, including (proto-)planetary nebulae and reflection nebulae. The MCs are presumably rich in fullerenes, whether they form from smaller hydrocarbons coagulating or the destruction of hydrogenated amorphous carbon dust (e.g. García-Hernández et al. 2011). In Galactic nebulae, fullerenes potentially take up 1 per cent of the elemental carbon abundance (Cami et al. 2010; Sellgren et al. 2010); as Table 2 shows, there is significantly more carbon available for fullerene formation in Magellanic objects. On average, García-Hernández et al.'s sample of Magellanic carbon-rich PNe contains 60 per cent more C_{60} than the Galactic PN, Tc-1. As a representative of large molecules, $C_{23}H_2$ is two orders of magnitude more abundant in

Magellanic carbon stars than in Galactic (Fig. 3) in our models. As a representative of cyclic molecules, benzene is $\sim$200 times more abundant in Magellanic carbon star envelopes than Galactic; its column density is $N(C_6H_6) \sim 10^{-5} N(C_2H_2)$.

These four molecules currently make up the extent of our knowledge of gas-phase species in the envelopes of carbon stars in the MCs. Given the derived line intensities and simulated spectra from Table 8 and Figs 7–8, ALMA will be able to detect a handful of molecules in a reasonable amount of time: detections of CO rotational lines will enable us to derive mass-loss rates and envelope expansion velocities; detections of other molecules will enable us to verify our chemical models, and to improve our understanding of circumstellar carbon chemistry at low metallicity.

7 SUMMARY

Driven by the recent interest in deep molecular absorption features in *Spitzer Space Telescope* spectra of evolved carbon stars in the MCs, we have conducted the first investigation into the circumstellar chemistry of carbon stars in three metallicity environments: that of the Galaxy (solar metallicity), the LMC (half solar metallicity) and the SMC (one-fifth solar metallicity). The general trend is that the abundances of hydrocarbons are greatly enhanced at low metallicity, so much so that the larger members of hydrocarbon families are more abundant than smaller members (e.g. C_6H_2 and C_8H_2 are more abundant than C_4H_2). At just half of solar metallicity, acetylene becomes more abundant in the CSE than carbon monoxide, the most abundant molecule apart from H_2 in Galactic CSEs. This is indicative of a suppressed oxygen chemistry at lower metallicity: other oxygen-bearing species are also less abundant. Nitrogen chemistry is also suppressed, except when it is incorporated into hydrocarbons (e.g. cyanopolyynes). This means that the main nitrogen repository in the envelope shifts from N_2 in Galactic stars to HCN in Magellanic stars. A similar trend is seen for heavy metals (e.g. Si), where SiC_2 behaves like a hydrocarbon, but other silicon-bearing molecules are rarer.

Physically, the lower expansion velocities of Magellanic CSEs mean that the envelopes are more dense. This implies that neutral–neutral reactions in the inner envelope are more rapid, but the stronger radiation fields in the LMC and SMC cause the molecular envelopes to be lesser in extent than in Galactic CSEs. The ionization fraction increases as metallicity drops, and the main charge carrier moves from a heavy metal (Mg^+) in Galactic envelopes to C^+.

We have compared the results from the Galactic model to the carbon star IRC+10216, and achieved reasonably good agreement in terms of molecular abundances and distributions. We discuss the qualitative results that have been obtained from infrared observations of carbon stars in the MCs, and also achieve good agreement, although constraints are few. Finally, we use our models to predict line intensities and images as seen by ALMA. ALMA is expected to improve our understanding of carbon stars in the MCs, and lines of CO, HCN, CS, CN, SiO and SiS should be detectable within 3 h of observation in LMC carbon stars. Lines of C_2H and ^{13}CO are predicted to be somewhat weaker, but may also be observable.

REFERENCES

Agúndez M. et al., 2010, A&A, 517, L2
Bernard J.-P. et al., 2008, AJ, 136, 919
Bieging J. H., Nguyen-Quang-Rieu, 1989, ApJ, 343, L25
Bieging J. H., Tafalla M., 1993, AJ, 105, 576
Bot C., Boulanger F., Lagache G., Cambrésy L., Egret D., 2004, A&A, 423, 567
Bouchet P., Lequeux J., Maurice E., Prevot L., Prevot-Burnichon M. L., 1985, A&A, 149, 330
Boyle R. J., Keady J. J., Jennings D. E., Hirsch K. L., Wiedemann G. R., 1994, ApJ, 420, 863
Cami J., Bernard-Salas J., Peeters E., Malek S. E., 2010, Sci, 329, 1180
Cernicharo J., Yamamura I., González-Alfonso E., de Jong T., Heras A., Escribano R., Ortigoso J., 1999, ApJ, 526, L41
Cernicharo J., Guélin M., Agúndez M., Kawaguchi K., McCarthy M., Thaddeus P., 2007, A&A, 467, L37
Cernicharo J., Guélin M., Agúndez M., McCarthy M. C., Thaddeus P., 2008, ApJ, 688, L83
Cernicharo J. et al., 2010, A&A, 521, L8
Cherchneff I., 2006, A&A, 456, 1001
Clayton G. C., Martin P. G., 1985, ApJ, 288, 558
Cordiner M. A., Millar T. J., 2009, ApJ, 697, 68
Decin L. et al., 2010, A&A, 518, L143
Dufour R. J., Shields G. A., Talbot R. J., Jr, 1982, ApJ, 252, 461
Elitzur M., Ivezić Ž., 2001, MNRAS, 327, 403
Ferrarotti A. S., Gail H.-P., 2006, A&A, 447, 553
Fonfría J. P., Cernicharo J., Richter M. J., Lacy J. H., 2008, ApJ, 673, 445
García-Hernández D. A. et al., 2011, ApJ, 737, L30
Gear C. W., 1971, Numerical Initial Value Problems in Ordinary Differential Equations. Prentice Hall, Englewood Cliffs, NJ
Gensheimer P. D., Likkel L., Snyder L. E., 1995, ApJ, 439, 445
Goldreich P., Scoville N., 1976, ApJ, 205, 144
Gordon K. D., Clayton G. C., Misselt K. A., Landolt A. U., Wolff M. J., 2003, ApJ, 594, 279
Gordon K. D. et al., 2009, ApJ, 690, L76
Groenewegen M. A. T., Oudmaijer R. D., Ludwig H.-G., 1997, MNRAS, 292, 686
Groenewegen M. A. T., Sloan G. C., Soszyński I., Petersen E. A., 2009, A&A, 506, 1277
Habing H. J., Tignon J., Tielens A. G. G. M., 1994, A&A, 286, 523
Hartquist T. W., Dalgarno A., Oppenheimer M., 1980, ApJ, 236, 182
Hasegawa T. I. et al., 2006, ApJ, 637, 791
He J. H., Dinh-V-Trung, Kwok S., Müller H. S. P., Zhang Y., Hasegawa T., Peng T. C., Huang Y. C., 2008, ApJS, 177, 275
Herbst E., Osamura Y., 2008, ApJ, 679, 1670
Höfner S., 2007, in Kerschbaum F., Charbonnel C., Wing R. F., eds, ASP Conf. Ser. 378, Why Galaxies Care about AGB Stars: Their Importance as Actors and Probes. Astron. Soc. Pac., San Francisco, p. 145
Hogerheijde M. R., van der Tak F. F. S., 2000, A&A, 362, 697
Huggins P. J., Glassgold A. E., 1982, ApJ, 252, 201
Ivezić Z., Elitzur M., 1996, MNRAS, 279, 1019
Jones A. P., 2001, Phil. Trans. R. Soc. Lond. A, 359, 1961
Jura M., Morris M., 1981, ApJ, 251, 181
Karakas A. I., 2010, MNRAS, 403, 1413
Karakas A. I., 2011, in Kerschbaum F., ed., ASP Conf. Ser., 445, Why Galaxies Care about AGB Stars II: Shining Examples and Common Inhabitants. Astron. Soc. Pac., San Francisco, p. 3
Kawaguchi K. et al., 2007, PASJ, 59, L47
Keady J. J., Ridgway S. T., 1993, ApJ, 406, 199
Keady J. J., Hall D. N. B., Ridgway S. T., 1988, ApJ, 326, 832
Kemper F., Stark R., Justtanont K., de Koter A., Tielens A. G. G. M., Waters L. B. F. M., Cami J., Dijkstra C., 2003, A&A, 407, 609

Koornneef J., 1982, A&A, 107, 247
Kwan J., Linke R. A., 1982, ApJ, 254, 587
Lagadec E. et al., 2007, MNRAS, 376, 1270
Lagadec E., Zijlstra A. A., Mauron N., Fuller G., Josselin E., Sloan G. C., Riggs A. J. E., 2010, MNRAS, 403, 1331
Leisenring J. M., Kemper F., Sloan G. C., 2008, ApJ, 681, 1557
Lequeux J., Maurice E., Prevot-Burnichon M.-L., Prevot L., Rocca-Volmerange B., 1982, A&A, 113, L15
Loup C., Forveille T., Omont A., Paul J. F., 1993, A&AS, 99, 291
Lucas R., Guélin M., Kahane C., Audinos P., Cernicharo J., 1995, Ap&SS, 224, 293
Mamon G. A., Glassgold A. E., Huggins P. J., 1988, ApJ, 328, 797
Markwick A. J., 2000, PhD thesis, UMIST
Marshall J. R., van Loon J. T., Matsuura M., Wood P. R., Zijlstra A. A., Whitelock P. A., 2004, MNRAS, 355, 1348
Matsuura M., Zijlstra A. A., van Loon J. T., Yamamura I., Markwick A. J., Woods P. M., Waters L. B. F. M., 2002, ApJ, 580, L133
Matsuura M. et al., 2005, A&A, 434, 691
Matsuura M. et al., 2006, MNRAS, 371, 415
Matsuura M. et al., 2008, in Kwok S., Sanford S. A., eds, Proc. IAU Symp. 251, Organic Matter in Space. Cambridge Univ. Press, Cambridge, p. 197
Matsuura M. et al., 2009, MNRAS, 396, 918
Mattsson L., Wahlin R., Höfner S., Eriksson K., 2008, A&A, 484, L5
Mattsson L., Wahlin R., Höfner S., 2010, A&A, 509, A14
Mauron N., 2008, A&A, 482, 151
McCarthy M. C., Gottlieb C. A., Gupta H., Thaddeus P., 2006, ApJ, 652, L141
Meixner M. et al., 2010, A&A, 518, L71
Men'shchikov A. B., Balega Y., Blöcker T., Osterbart R., Weigelt G., 2001, A&A, 368, 497
Millar T. J., 2008, Ap&SS, 313, 223
Millar T. J., Herbst E., 1994, A&A, 288, 561
Millar T. J., Herbst E., Bettens R. P. A., 2000, MNRAS, 316, 195
Millar T. J., Walsh C., Cordiner M. A., Ní Chuimín R., Herbst E., 2007, ApJ, 662, L87
Monnier J. D., Danchi W. C., Hale D. S., Tuthill P. G., Townes C. H., 2000, ApJ, 543, 868
Müller H. S. P., Thorwirth S., Roth D. A., Winnewisser G., 2001, A&A, 370, L49
Müller H. S. P., Schlöder F., Stutzki J., Winnewisser G., 2005, J. Mol. Struct., 742, 215
Olofsson H., 2008a, Ap&SS, 313, 201
Olofsson H., 2008b, Phys. Scr., 133, 014028
Paladini R., Montier L., Giard M., Bernard J. P., Dame T. M., Ito S., Macias-Perez J. F., 2007, A&A, 465, 839
Remijan A. J., Hollis J. M., Lovas F. J., Cordiner M. A., Millar T. J., Markwick-Kemper A. J., Jewell P. R., 2007, ApJ, 664, L47
Sandstrom K. M., Bolatto A. D., Draine B. T., Bot C., Stanimirović S., 2010, ApJ, 715, 701
Sandstrom K. M. et al., 2012, ApJ, 744, 20
Scalo J. M., Slavsky D. B., 1980, ApJ, 239, L73
Schaefer B. E., 2008, AJ, 135, 112
Schöier F. L., Olofsson H., 2001, A&A, 368, 969
Schöier F. L., van der Tak F. F. S., van Dishoeck E. F., Black J. H., 2005, A&A, 432, 369
Schöier F. L., Fong D., Olofsson H., Zhang Q., Patel N., 2006, ApJ, 649, 965
Schöier F. L., Fong D., Bieging J. H., Wilner D. J., Young K., Hunter T. R., 2007a, ApJ, 670, 766
Schöier F. L., Bast J., Olofsson H., Lindqvist M., 2007b, A&A, 473, 871
Sellgren K., Werner M. W., Ingalls J. G., Smith J. D. T., Carleton T. M., Joblin C., 2010, ApJ, 722, L54
Sharp C. M., Huebner W. F., 1990, ApJS, 72, 417
Sloan G. C., Kraemer K. E., Matsuura M., Wood P. R., Price S. D., Egan M. P., 2006, ApJ, 645, 1118
Sloan G. C. et al., 2009, Sci, 323, 353
Speck A. K., Cami J., Markwick-Kemper C., Leisenring J., Szczerba R., Dijkstra C., Van Dyk S., Meixner M., 2006, ApJ, 650, 892
Szewczyk O., Pietrzyński G., Gieren W., Ciechanowska A., Bresolin F., Kudritzki R.-P., 2009, AJ, 138, 1661
Tanabé T. et al., 1997, Nat, 385, 509
Thaddeus P., Gottlieb C. A., Gupta H., Brünken S., McCarthy M. C., Agúndez M., Guélin M., Cernicharo J., 2008, ApJ, 677, 1132
Tsuji T., 1964, Ann. Tokyo Astron. Obser., 9, 1
Tsuji T., 1973, A&A, 23, 411
van den Bergh S., 1968, J. R. Astron. Soc. Canada, 62, 219
van Genderen A. M., 1970, A&A, 7, 49
van Loon J. T., 2000, A&A, 354, 125
van Loon J. T., 2006, in Lamers H. J. G. L. M., Langer N., Nugis T., Annuk K., eds, ASP Conf. Ser. 353, Stellar Evolution at Low Metallicity: Mass Loss, Explosions, Cosmology. Astron. Soc. Pac., San Francisco, p. 211
van Loon J. T., Zijlstra A. A., Groenewegen M. A. T., 1999a, A&A, 346, 805
van Loon J. T., Groenewegen M. A. T., de Koter A., Trams N. R., Waters L. B. F. M., Zijlstra A. A., Whitelock P. A., Loup C., 1999b, A&A, 351, 559
van Loon J. T., Marshall J. R., Matsuura M., Zijlstra A. A., 2003, MNRAS, 341, 1205
van Loon J. T., Cohen M., Oliveira J. M., Matsuura M., McDonald I., Sloan G. C., Wood P. R., Zijlstra A. A., 2008, A&A, 487, 1055
Wachter A., Winters J. M., Schröder K.-P., Sedlmayr E., 2008, A&A, 486, 497
Wahlin R., Eriksson K., Gustafsson B., Hinkle K. H., Lambert D. L., Ryde N., Westerlund B., 2006, Mem. Soc.Ã Astron. Italiana, 77, 955
Wallerstein G., Knapp G. R., 1998, ARA&A, 36, 369
Westerlund B. E., 1997, The Magellanic Clouds. Cambridge Univ. Press, New York, p. 234
Willacy K., Cherchneff I., 1998, A&A, 330, 676
Winters J. M., Le Bertre T., Jeong K. S., Helling C., Sedlmayr E., 2000, A&A, 361, 641
Woitke P., 2006, A&A, 460, L9
Wood P. R., Habing H. J., McGregor P. J., 1998, A&A, 336, 925
Woodall J., Agúndez M., Markwick-Kemper A. J., Millar T. J., 2007, A&A, 466, 1197
Woods P. M., Schöier F. L., Nyman L.-Å., Olofsson H., 2003, A&A, 402, 617
Woods P. M. et al., 2011, MNRAS, 411, 1597
Zhang Y., Kwok S., 2011, ApJ, 730, 126
Zijlstra A. A. et al., 2006, MNRAS, 370, 1961

SUPPORTING INFORMATION

Additional Supporting Information may be found in the online version of this article:

Figs 9–32. Line profiles of each line transition.

Please note: Wiley-Blackwell are not responsible for the content or functionality of any supporting materials supplied by the authors. Any queries (other than missing material) should be directed to the corresponding author for the article.

This paper has been typeset from a TEX/LATEX file prepared by the author.